Acid-Catalysed Furfural Conversion: Enhanced Kinetic Insights into Formic Acid and Humin

Chandra Wendy Handriono [a,1], I Gede Pandega Wiratama [a,2], Nicholas Chandra [a,3], H.J. Heeres [b,4], Jenny Novianti Muliarahayu Tan-Soetedjo [a,5,*]

[a] Center of Renewable Energy Conversion, Department of Chemical Engineering, Faculty of Engineering Technology, Parahyangan Catholic University, Bandung, Indonesia
[b] Green Chemical Reaction Engineering, Engineering & Technology Institute Groningen, University of Groningen, Groningen, Netherlands
[1] chandrawendy13@gmail.com; [2] pandega.wiratama@unpar.ac.id; [3] nicholaschandra.main01@gmail.com; [4] h.j.heeres@rug.nl;
[5] jenny.novianti@unpar.ac.id *
* corresponding author

ARTICLE INFO

Article history
Received November 11, 2025
Revised December 16, 2025
Accepted December 19, 2025

Keywords
Biorefinery
Formic Acid
Furfural
Humins
Kinetic Study

ABSTRACT

Furfural is a key platform molecule derived from lignocellulosic biomass and an essential precursor for biofuels, chemicals, and polymer materials. Its stability under acidic hydrothermal conditions critically affects biomass conversion efficiency. While numerous studies have explored furfural formation and xylose conversion, a comprehensive kinetic model that quantitatively captures furfural degradation pathways—particularly to formic acid and humins—and their interactions remains limited. This study addresses this gap by evaluating multiple kinetic models to identify the most accurate representation of furfural conversion behavior and by determining detailed kinetic parameters. Experiments were performed by reacting furfural with sulfuric acid at 140-180°C using furfural concentrations of 0.05–0.63 M and acid concentrations of 0.05-1.00 M. Among the tested models, Model 3 showed the highest predictive accuracy, with R^2 values of 98.04% for furfural conversion and 90.35% for formic acid formation. The estimated activation energies (Ea_1 = 107.84 ± 0.53 kJ mol^{-1}, Ea_2 = 81.75 ± 0.76 kJ mol^{-1}, and Ea_4 = 117.07 ± 0.96 kJ mol^{-1}) indicate that humin formation has the lowest energetic barrier. In contrast, the autocatalytic formation of formic acid becomes significant only at elevated temperatures. Reaction orders of 0.81 for furfural, 0.62 for sulfuric acid, and 1.49 for formic acid reveal that both catalytic acidity and autocatalysis govern the overall reaction rate. Operational conditions strongly influence product selectivity: higher acid and furfural concentrations accelerate reactions but promote humin formation, whereas lower concentrations favor formic acid production. Overall, this study provides a holistic kinetic framework that accurately predicts the behavior of key species, offering valuable insights for reactor design and process optimization in furfural-based biorefineries.

1. Introduction

As the transition towards a low-carbon chemical industry accelerates globally, furfural derived from lignocellulosic biomass has emerged as a strategically crucial renewable platform chemical. Lignocellulosic biomass is widely recognised as a cornerstone of sustainable resource utilisation due to its abundance in agricultural, forestry, and industrial residues, its non-competition with food supply chains, and its high polysaccharide content. Among these residues, empty fruit bunches from the Indonesian palm oil industry are among the most accessible and hemicellulose-rich feedstocks in Southeast Asia [1], [2]. The structural composition of lignocellulosic biomass enables the valorisation

of cellulose, hemicellulose, and lignin into high-value products, with hemicellulose-derived pentoses serving as key precursors for furfural. Owing to its molecular versatility, furfural plays a central role in the production of renewable fuels, solvents, polymer resins, and a wide range of industrial chemicals [3], [4], [5], [6].

Despite its strategic significance, furfural production remains constrained by the compound's inherent chemical instability during conversion. Under aqueous acidic and elevated-temperature conditions, furfural readily undergoes rehydration, fragmentation, and condensation reactions that generate formic acid and humins. These conversion pathways not only diminish furfural yields but also influence reaction selectivity, carbon utilisation efficiency, and operational reliability, particularly through humin-induced reactor fouling and catalyst deactivation [7], [8], [9]. As the balance between furfural formation and conversion is sensitive to reaction conditions, a refined mechanistic understanding of its behaviour in reactive media is essential for advancing more efficient and sustainable production processes.

Although significant progress has been made in elucidating individual reaction mechanisms, a critical research gap persists: no fully integrated kinetic framework has yet described the furfural conversion. Many studies provide valuable insight into specific reaction steps, yet they do not collectively offer a comprehensive mechanistic picture of furfural chemistry under practical processing conditions [10], [11], [12], [13], [14]. The fundamental gap is not simply a limited number of investigations but the absence of a quantitatively robust and integrated kinetic model capable of simultaneously describing the principal conversion pathways and the dynamic interplay that governs their competition. Existing kinetic models generally isolate individual pathways, regard furfural as a stable final product, or quantify only selected reactions without considering their interdependence [8], [14], [15]. These fragmented approaches inhibit the ability to quantify how reaction conditions influence competing pathways, prevent accurate prediction of realistic furfural yields, and restrict the development of optimisation-driven strategies required for industrial implementation. Consequently, the lack of an integrated mechanistic framework constitutes a significant barrier to advancing both scientific understanding and technological innovation in biomass-derived furfural production.

The approach adopted in this study and the novelty it introduces lie in the development of a unified, mechanistically explicit kinetic model that captures the full complexity of furfural conversion in aqueous sulphuric acid while concurrently providing holistic quantification of formic acid and humin formation. This integrated framework consolidates the principal conversion pathways into a single, quantitatively validated system capable of describing their interactions across a broad range of reaction conditions. By offering a comprehensive kinetic description that predicts the temporal evolution of key species and elucidates the intrinsic competition governing furfural stability, the model provides a mechanistically grounded tool for identifying process limitations, optimising reaction conditions, and guiding the design of more selective conversion strategies. This advancement strengthens the scientific foundation needed to accelerate the development of economically viable, environmentally sustainable technologies for producing furfural.

2. Research Methodology

2.1. Materials

The materials used in this experiment included furfural (99% purity), concentrated sulphuric acid (95-97%wt) obtained from Merck Life Science N.V., and formic acid (98% purity) obtained from Sigma-Aldrich Chemie GmbH. All chemicals were used as received without further purification. Deionized water was used to prepare all solutions.

2.2. Procedures

All reactions were conducted in glass ampoules with an inner diameter of 3 mm, a wall thickness of 1.5 mm, and a length of 150 mm. Each ampoule was filled at room temperature with a 0.5 cm^3 solution of furfural and sulfuric acid, and then sealed tightly using a torch. The sealed ampoules were placed on a rack and put in a constant-temperature oven (±0.1°C) set to the desired reaction temperature. After the specified reaction time, an ampoule was removed from the oven and immediately quenched in a cold-water bath. The liquid contents were then filtered using a PTFE syringe filter (0.45 µm, VWR, the Netherlands). The particle-free aliquot was subsequently diluted 7-8 times with water before HPLC analysis.

2.3. Analytical Methods

The liquid phase composition was characterised using an Agilent 1200 HPLC system equipped with an Agilent 1200 pump, a Bio-Rad Aminex HPX-87H organic acid column, and dual UV and RID detectors. The mobile phase consisted of 5 mm aqueous sulphuric acid, delivered at a flow rate of 0.55 $cm^3.min^{-1}$, with the column held at 60°C. Each analysis was completed within 60 minutes, and a representative chromatogram is shown in Fig. 1. As illustrated in Fig.1., in addition to sulphuric acid (SA) and furfural (F), both of which were present before the reaction, a distinct peak corresponding to formic acid (FA) appeared and increased substantially after a specific reaction time. The concentrations of the individual compounds in the product mixture were quantified using calibration curves constructed from standard solutions of known concentrations.

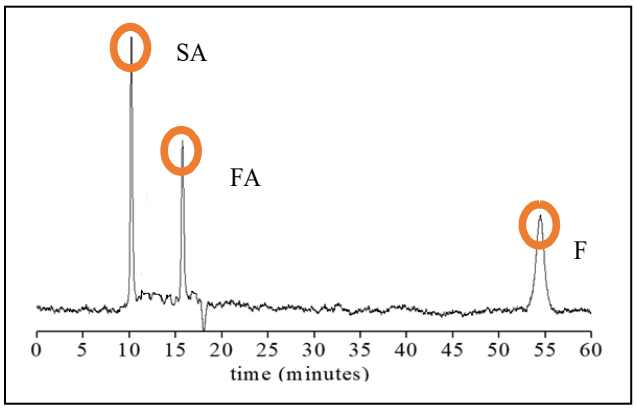

Fig. 1. Representative HPLC Chromatogram for Furfural Decomposition (F = Furfural; FA = Formic Acid; SA = Sulphuric Acid)

2.4. Heat Transfer Coefficient Assessment in the Oven

At reaction start-up, the system experiences a transient, non-isothermal phase as the ampoule contents warm from room temperature to the set oven temperature. To characterise the heating period and its effect on the kinetic modelling, the temperature trajectories within the ampoules were determined experimentally. In this procedure, an ampule containing a representative solvent and equipped with a thermocouple was placed in the oven, and the temperature variation over time was recorded.

The measurement was repeated across several oven temperatures, and the resulting profiles were analysed using a heat balance to capture the thermal dynamics of the ampoule system.

$$\frac{d(mCpT)}{dt} = UA(T_{oven} - T) \tag{1}$$

$$\frac{dT}{dt} = \frac{UA}{mCp}(T_{oven} - T) = h(T_{oven} - T) \tag{2}$$

$$T = T_{oven} - (T_{oven} - T_0) \cdot e^{-ht} \tag{3}$$

Solving the ordinary differential equation (2) under the initial condition t = 0. T = Ti gives:

$$T = T_{oven} - (T_{oven} - T_i) \cdot e^{-ht} \tag{4}$$

To represent the transient non-isothermal regime during the early stage of the reaction, equation (4) was included in the kinetic formulation. The heat transfer coefficient (h) was estimated by regressing the experimental temperature-time profiles against equation (5). The temperature dependence was derived by fitting the calculated h-values at oven set points between 140°C and 180°C and was adequately described by a simpler linear relationship.

$$h(T) = 0.0015\left(T - T_{ref}\right) + 0.3182 \quad (5)$$

2.5. Definitions

The conversion of furfural (XF) and the yield of formic acid (YFA) are defined by equations (6) and (7) and are expressed on a %-mol basis.

$$X_F = \frac{C_{F,0} - C_{F,t}}{C_{F,0}} \quad (6)$$

$$Y_{FA} = \frac{C_{FA,t} - C_{FA,0}}{C_{FA,0}} \quad (7)$$

2.6. Determination of the Kinetic Parameters

The model equations were implemented in MATLAB. The system of ordinary differential equations (ODEs) was numerically integrated using ODE23s. Kinetic parameters were estimated by a nonlinear least-squares method using the MATLAB function lsqnonlin, which employs the Trust-Region Reflective algorithm, minimizing the error between model predictions and experimental data.

3. Results and Discussion

3.1. Screening Studies

A total of 28 experiments were carried out over the temperature range of 140-180°C, using initial furfural concentrations ($C_{F,0}$) of 0.05-0.63 M and sulphuric acid concentrations (CSA) of 0.05-1.00 M in an aqueous medium. As a result, formic acid (FA) and humins were identified as products of furfural conversion. A representative concentration–time profile is presented in Fig. 2.

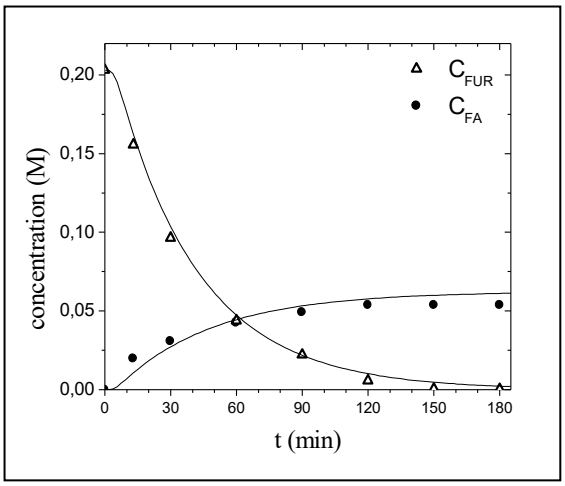

Fig. 2. Typical concentration profile of furfural conversion (T = 162°C, $C_{F,0}$ = 0.20 M, C_{SA}= 0.50 M)

Screening experiments were carried out to evaluate the influence of acid strength and temperature on the conversion of furfural and the formation of formic acid under aqueous acidic conditions, with the results summarised in Fig. 3. and Fig. 4. Across all conditions, the concentration profiles of furfural display exponential decay, indicating pseudo–first-order kinetics consistent with established descriptions of acid-catalysed furanic conversion where the catalyst and solvent remain in significant excess. In Fig. 3, increasing the concentration of sulphuric acid (CSA) leads to a pronounced increase in the observed rate of furfural depletion and a faster rate of formic acid formation, confirming the catalytic role of Brønsted acidity in promoting the primary transformation steps [9], [16]. Nevertheless, the final concentration of formic acid does not increase proportionally with CSA loading, suggesting that strongly acidic conditions intensify secondary pathways, including

condensation, polymerisation, and potential conversion of formic acid, which ultimately restricts the achievable carbon efficiency. This interpretation is further reinforced by the trends in Fig. 4, where raising the temperature from 140°C to 180°C at constant CSA accelerates furfural depletion and enhances the early formation of formic acid. However, the product concentration subsequently approaches a steady limit region at higher temperatures. The emergence of this steady-limit behaviour aligns with reports of formic acid. However, a principal fragmentation product of furfural may undergo subsequent reactions or participate in condensation networks in harsh hydrothermal environments [8], [17], [18]. Taken together, Fig. 3 and Fig. 4 provide consistent mechanistic evidence that both acidity and temperature substantially increase the reaction rate while simultaneously intensifying undesired side reactions under overly severe conditions [7], [8]. These observations establish a foundational rationale for identifying an operational window that balances rapid furfural activation with controlled selectivity, and they confirm the suitability of the dataset for the kinetic modelling and optimisation analyses presented later in the present study.

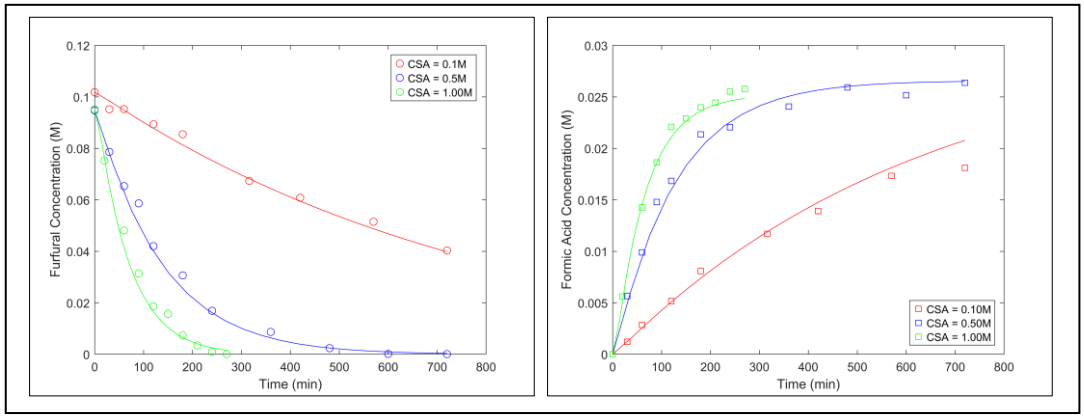

Fig. 3. Effect of sulphuric acid concentration on furfural conversion (left) and formic acid formation (right) at constant temperature (T = 142°C)

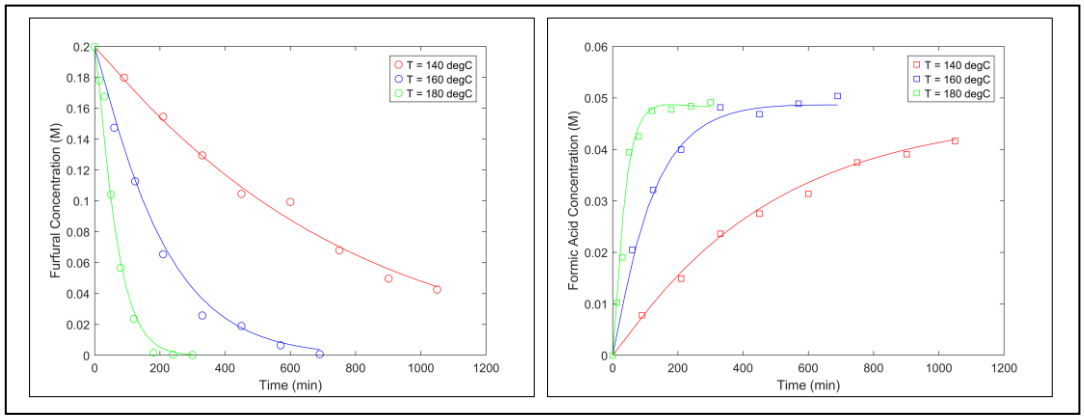

Fig. 4. Effect of reaction temperature on furfural conversion (left, ○) and formic acid formation (right, □) at constant sulphuric acid concentration (C_{SA}= 0.10 M)

3.2. Model Approaches

A total of 28 experiments with more than 225 data points in a temperature window of 140-180°C using initial furfural concentrations ($C_{F,0}$) between 0.05 and 0.63 M with water solvent. The kinetic modelling results reveal that furfural decomposition in an aqueous medium catalysed by sulphuric acid proceeds through competitive pathways leading to the formation of formic acid and humins. Unlike previous studies that mainly focused on furfural formation, this work emphasises the importance of furfural conversion reactions in governing overall selectivity and yield. The application of a power-law kinetic framework enabled the quantitative description of furfural conversion and by-product formation, providing deeper insight into the reaction kinetics and the stability of furfural under acidic aqueous conditions. These results contribute to a more comprehensive understanding of the complex reaction network involved in biomass-derived furfural processing. The catalytic role of sulfuric acid in this system can be interpreted as follows, equation (8) [7], [19]:

$$C_{H^+} = C_{H_2SO_4} + \frac{1}{2}\left(-K_{a,HSO_4^-} - C_{H_2SO_4} + \sqrt{\left(K_{a,HSO_4^-} + C_{H_2SO_4}\right)^2 + 4C_{H_2SO_4}K_{a,HSO_4^-}}\right) \quad (8)$$

Where $K_{a,HSO4}^-$ is the dissociation constant of HSO_4^- which was calculated using equation (9).

$$K_{a,HSO_4}{}^- = 10^{-p_{Ka}} \quad (9)$$

Here the $P_{K\alpha}$ is calculated using equation 10, with a correction for the mixture's temperature (T).

$$p_{Ka} = 0.0152T - 2.636 \quad (10)$$

The reaction rate for each substance can be generalized as in equation 11:

$$R_i = k_i(C_{substance})^{an}(C_{H^+})^{an} \quad (11)$$

3.3. Kinetic Modelling Development

Three kinetic models were evaluated to examine the possible pathways of furfural decomposition in an aqueous medium catalysed by sulphuric acid. Each model represents a different assumption regarding the formation of formic acid and humins [8], [9], [17], [20]. The comparison aims to identify which model best fits the experimental data and provides the most representative kinetic parameters.

1) Model-1

The first model represents a straightforward reaction scheme consisting of two main steps: (i) furfural was converted partially into formic acid, and (ii) the rest polymerised, forming humins, as illustrated in Fig. 5. Model-1 is the simplest proposed model in this study.

The preceding model yields the mass-balance expressions for the individual components in the batch reactor, which are given in equation (12) and (13):

$$\frac{dC_f}{dt} = -R_1 - R_2 \quad (12)$$

$$\frac{dC_{FA}}{dt} = R_1 \quad (13)$$

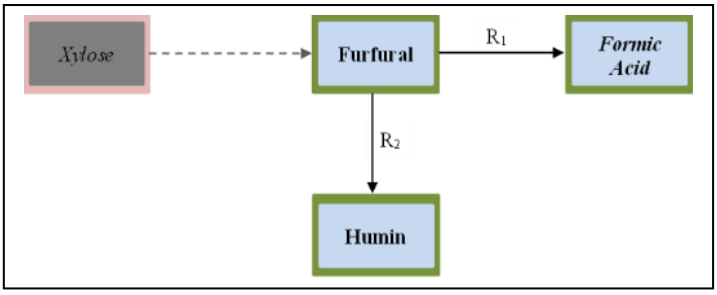

Fig. 5. Direct furfural decomposition without consecutive reactions

The reaction rate was modelled using a power-law approach, see equation (14) for details.

$$R_i = k_i(C_F)^{\beta i} \quad (14)$$

The temperature dependence of the kinetic constants was described by a modified Arrhenius relationship, as shown in equation (15), with C_{H^+} calculation that is shown in equation (8) above.

$$k_i = k_{i0}(C_{H^+})^{\alpha i} exp\left(\frac{-Eai}{R}\left(\frac{1}{T_{real}} - \frac{1}{T_{ref}}\right)\right) \quad (15)$$

In this equation, T is the reaction temperature, and Tref is the reference temperature, set at 142°C for this study in acid-catalysed conditions. The corresponding kinetic parameter values are shown in Table 1. According to Fig. 6, furfural concentration decreases steadily over time, and this decline becomes faster at higher temperatures or higher acid concentrations. In contrast, formic acid accumulates progressively as furfural decomposes, with its formation rate also enhanced under more acidic conditions or at higher temperatures. Overall, the experimental concentration profiles agree well with the model.

Table 1. Kinetic Parameters for Model-1

Parameter	Unit	Value ± deviation	Parameter	Value ± deviation
$k_{1,0}$	L mol^{-1} min^{-1}	8.28 x 10^{-3} ± 0.001	α_1	0.97 ± 0.039
$k_{2,0}$	L mol^{-1} min^{-1}	4.12 x 10^{-2} ± 0.004	β_1	0.83 ± 0.055
Ea_1	kJ mol^{-1}	109.17 ± 4.38	α_2	0.98 ± 0.028
Ea_2	kJ mol^{-1}	86.97 ± 2.94	β_2	1.10 ± 0.032
$R^2_{X_F}$	%	97.85		
$R^2_{Y_{FA}}$	%	88.84		

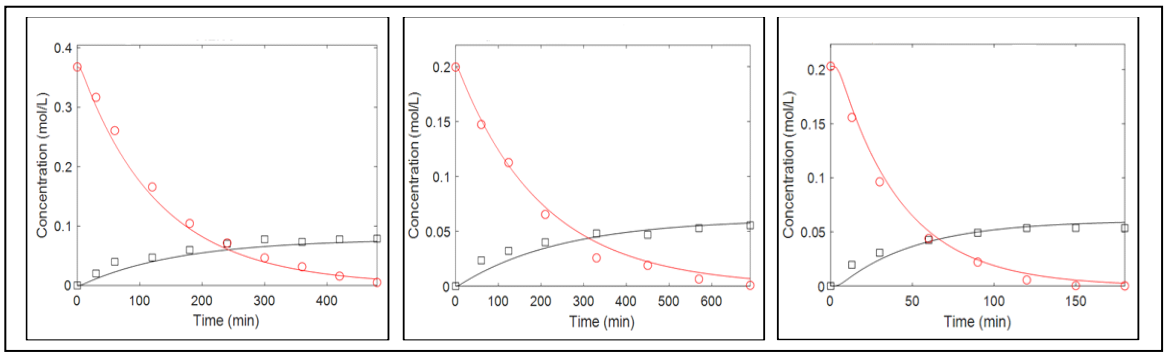

Fig. 6. Typical reaction profile of the acid-catalysed furfural decomposition at different temperatures for Model-1 (left → T = 142°C with C_{SA} = 0.50 M; middle → T = 162°C with C_{SA} = 0.10 M; right → T = 162°C with C_{SA} = 0.05 M)

2) Model-2

To obtain the most representative model with the best-fitting kinetic parameters, a comparison was made by considering alternative reaction pathways that may occur during furfural decomposition, as shown in Fig. 7. This model extends Model-1 by assuming that the formic acid produced from furfural undergoes a subsequent reaction leading to the formation of additional by-products [21], [22]. Equations (14) and (16) give the mass balances for furfural and formic acid in a batch reactor under Model-2.

$$\frac{dC_{FA}}{dt} = R_1 - R_3 \quad (16)$$

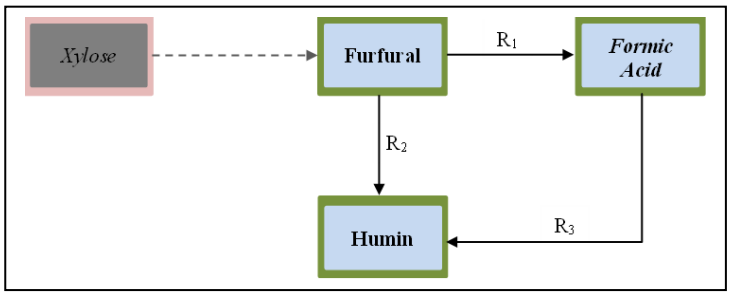

Fig. 7. Formation of formic acid from furfural with subsequent reaction

The kinetic parameters for Model-2 are shown in Table 2. The results obtained from Model-2 did not differ significantly from those of Model-1.

Table 2. Kinetic parameters for Model-2.

Parameter	Unit	Value ± deviation	Parameter	Value ± deviation
$k_{1,0}$	L mol^{-1} min^{-1}	8.85 x 10^{-3} ± 0.0018	α_1	0.98 ± 0.041
$k_{2,0}$	L mol^{-1} min^{-1}	4.27 x 10^{-2} ± 0.0052	β_1	0.81 ± 0.061
$k_{3,0}$	L mol^{-1} min^{-1}	5.52 x 10^{-4} ± 0.0006	α_2	0.98 ± 0.032
Ea_1	kJ mol^{-1}	102.63 ± 6.16	β_2	1.13 ± 0.043
Ea_2	kJ mol^{-1}	89.36 ± 3.90	α_3	1.15 ± 0.351
Ea_3	kJ mol^{-1}	7.67 ± 2.73	β_3	0.66 ± 0.292
$R^2_{X_F}$	%	97.89		
$R^2_{Y_{FA}}$	%	88.89		

3) Model-3

Although Model-2 yields higher R^2 values than Model-1, its kinetic parameters exhibit greater variability, suggesting that both models fail to capture a key reaction pathway. To overcome this limitation, Model-3 was developed as an extended framework informed by the preceding models. This scheme explicitly accounts for the further reaction of formic acid, produced during furfural decomposition, with furfural to form additional by-products as shown in Fig. 8 [8], [17], [21].

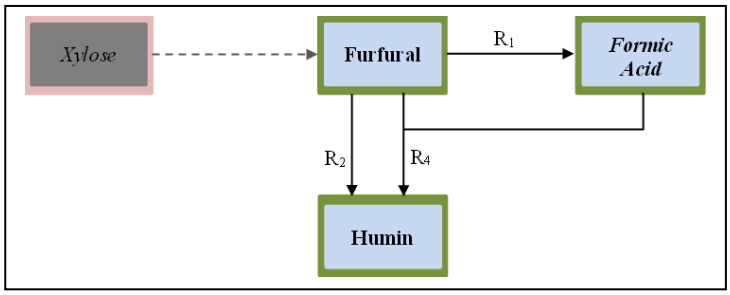

Fig. 8. Combination model between model-1 and model-3

For Model-3, the mass balances for furfural and formic acid in the batch reactor are given by equations (16) and (17).

$$\frac{dC_{FA}}{dt} = R_1 - R_4 \tag{17}$$

Unlike the mass-balance expressions in Models 1 and 2, in this model, the reaction rate R_4 is influenced by two components, namely furfural and formic acid. Accordingly, the mass-balance equations for furfural and formic acid are expressed as given in equation (18).

$$R_4 = k_4(C_F)^{\beta 4}(C_{FA})^{\gamma 4} \tag{18}$$

The same procedure was subsequently applied to determine the kinetic parameters, with the results reported in Table 3.

Table 3. Kinetic Parameters for Model-3

Parameter	Unit	Value ± deviation	Parameter	Value ± deviation
$k_{1,0}$	L mol^{-1} min^{-1}	1.43 x 10^{-2} ± 0.0007	α_1	0.92 ± 0.006
$k_{2,0}$	L mol^{-1} min^{-1}	2.98 x 10^{-2} ± 0.0015	β_1	0.97 ± 0.008
$k_{4,0}$	L mol^{-1} min^{-1}	2.65 x 10^{-1} ± 0.011	α_2	1.09 ± 0.009
Ea_1	kJ mol^{-1}	107.84 ± 0.53	β_2	1.01 ± 0.009
Ea_2	kJ mol^{-1}	81.75 ± 0.76	α_4	0.62 ± 0.011
Ea_4	kJ mol^{-1}	117.07 ± 0.96	β_4	0.81 ± 0.007
$R^2_{X_F}$	%	98.04	γ_4	1.49 ± 0.008
$R^2_{Y_{FA}}$	%	90.35		

3.4. Determination of the Best-Performing Model

As shown in Table 4, all models exhibit high R^2 values for furfural conversion and formic acid formation. For furfural conversion, R^2 values were 97.85% (Model-1), 97.89% (Model-2), and 98.04% (Model-3), while for formic acid yield, they were 88.84%, 88.89%, and 90.35%, respectively. Although the differences are modest, Model-3 consistently achieved the highest R^2 values. However, as R^2 alone may favour more complex models, AIC was applied to account for model complexity. Model-3 showed the lowest AIC value (–556.75), compared with –546.83 for Model-1 and –541.63 for Model-2, indicating the most favourable balance between goodness-of-fit and simplicity. Consequently, the combined R^2 and AIC analysis confirms Model-3 as the most statistically robust model, with improved performance not attributable to overfitting [23], [24], [25].

Table 4. R^2 value for furfural conversion and formic acid yield

Model	AIC	$R^2_{X_F}$	$R^2_{Y_{FA}}$
1	-546.83	97.85	88.84
2	-541.63	97.89	88.89
3	-556.75	98.04	90.35

Additional validation was provided by a parity plot, which visually compares predicted and experimental concentrations. A high-performing model is characterised by data points that cluster closely along the 45° diagonal line. As shown in Fig. 9, the slightly greater variability observed in the parity plot for formic acid, regardless of the model, suggests the inherent complexity of its formation pathways, which involve nonlinear reactions and humin formation. Even under these challenging conditions, Model-3 delivers the highest consistency and stability in predicting formic acid concentrations, reinforcing its status as the most realistic and reliable model.

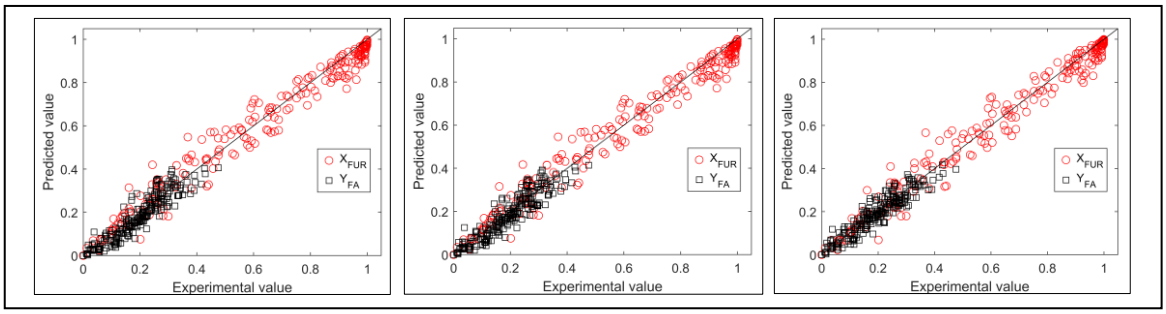

Fig. 9. Parity plot (left: model-1; middle: model-2; right: model-3; ○ furfural, □ formic acid)

In summary, the convergence of statistical evidence (higher R^2 and lowest AIC), improved residual error performance, and strong mechanistic justification collectively confirm that Model-3 is the best-performing kinetic model for describing furfural conversion and formic acid formation under the studied reaction conditions [9], [24], [26].

3.5. Kinetic Implications of Furfural Conversion

Activation energy (Ea) defines the kinetic barrier of each reaction pathway and reflects both the reaction mechanism and its temperature sensitivity in furfural conversion. As shown in Fig. 10, the Ea for furfural conversion to formic acid, Ea1, ranges from 102.63 to 109.17 kJ mol^{-1}. Among the three models, Model-3 provides the most reliable estimate of 107.84 ± 0.52 kJ mol^{-1}, indicating a well-constrained and stable kinetic description with lower uncertainties than those observed in Models 1 and 2. For humin formation directly from furfural Ea_2, activation energies lie between 81.75 and 89.36 kJ mol^{-1}. Model-3 again exhibits the lowest deviation of 81.75 ± 0.75 kJ mol^{-1}, confirming that humin formation is kinetically more favourable than formic acid production. Differences between the models become evident in secondary humin pathways. Model-2 includes a very low and poorly constrained Ea_3 of 7.67 ± 2.73 kJ mol^{-1} for the conversion of formic acid into humin precursors, whereas Model-3 incorporates a furfural–formic acid condensation step characterised by a substantially higher Ea_4 of 117.07 ± 0.96 kJ mol^{-1}. This higher barrier is consistent with the significant energetic requirements of C–C and C–O bond formation during polycondensation processes [27], [28], [29]. The participation of formic acid in these secondary reactions indicates that it functions not only as a reaction product but also as an active contributor to the acidic environment, thereby promoting acid-mediated rearrangement, condensation, and cross-linking reactions [12], [17], [21],

[30], [31]. The consistently low uncertainties and strong mechanistic coherence of Ea_1, Ea_2, and Ea_4 demonstrate that Model-3 provides the most internally consistent and physically meaningful kinetic representation.

Fig. 10 further confirms that the activation energies derived from Model-3 fall within established experimental ranges, indicating realistic kinetics rather than overfitting. Specifically, the values of Ea_1, Ea_2, and Ea_4 in the range 81.75 to 117.07 kJ mol^{-1} are well within those reported in previous studies [13], [14], [15], [17], [30], [32], [33], [34], where activation energies for furfural conversion reactions can reach up to approximately 125.10 kJ mol^{-1} [32]. Notably, Model-3 values closely overlap with literature data for oxidation, carbonyl transformation, polymerisation, and condensation reactions involving furanic intermediates. Higher activation energies associated with humin formation reflect the substantial energy demands of cross-polymerisation. At the same time, lower values in the range of 44.16 to 93.02 kJ mol^{-1} are characteristic of acid-catalysed conversion steps. This close agreement between experimental trends, mechanistic interpretation, and literature data reinforces the robustness and credibility of the proposed kinetic framework.

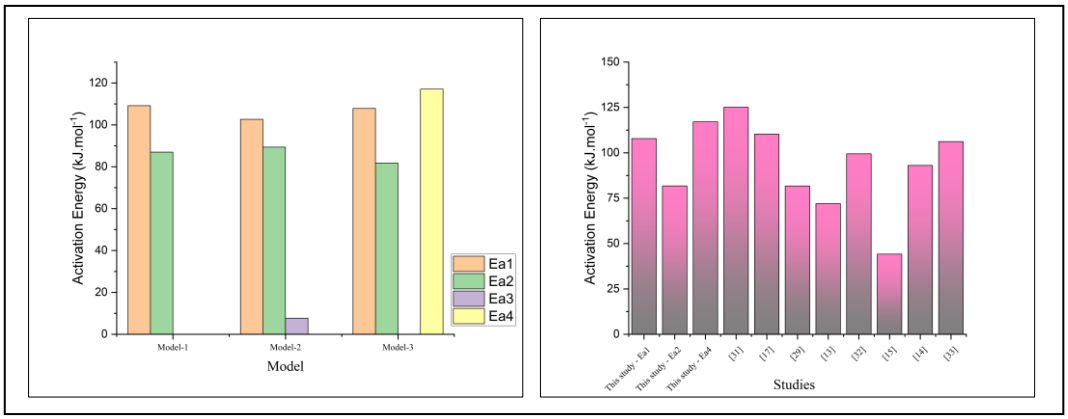

Fig. 10. Comparison of activation energy (Ea) for each model (left) and comparison of activation energy for several studies (right)

The reaction-order analysis reported in Table 5 provides quantitative insight into the kinetic sensitivity of furfural conversion to changes in acid concentration and reaction pathways. Proton reaction orders (α), which predominantly fall within the range 0.92-1.13, demonstrate that acidity is the principal kinetic driver of the system [30]. Values close to unity indicate an almost proportional increase in reaction rate with increasing acid concentration, highlighting a high sensitivity of the kinetics to proton availability. Slightly sub-unity values suggest partial saturation of protonation sites or buffering effects, which moderate the kinetic response to further increases in acidity. Conversely, α values exceeding unity indicate enhanced sensitivity, in which small increases in acid concentration result in a disproportionately large acceleration of the reaction, consistent with the involvement of multiple proton-dependent steps. The reaction orders with respect to furfural (β), as listed in Table 5, span 0.66-1.13 and reflect varying degrees of substrate participation in the rate-determining step. Near-unity values imply direct involvement of furfural, whereas lower values indicate rapid pre-equilibria or intermediate formation that reduce the apparent kinetic influence of substrate concentration. A distinctive behaviour is observed in Model-3, where the reaction order for formic acid ($\gamma = 1.49$) indicates a strong super-linear kinetic response. This pronounced sensitivity confirms that formic acid acts as an active co-catalyst, enhancing proton transfer and stabilising protonated intermediates, thereby introducing cooperative acid-controlled kinetics [17], [27], [35]. The consistency between the reaction orders in Table 5 and the corresponding activation energies supports a multistep, acid-dependent reaction network. Pathways that are highly sensitive to acid concentration tend to exhibit lower energetic barriers, whereas routes with higher activation energies remain intrinsically demanding despite strong acid participation. Overall, the kinetic parameters demonstrate that acid concentration critically governs both reaction rate and pathway accessibility in furfural conversion.

Table 5. Reaction order for all models

Model	α_1	β_1	α_2	β_2	α_3	β_3	α_4	β_4	γ_4
1	0.97	0.83	0.98	1.10					
2	0.98	0.81	0.98	1.13	1.15	0.66			
3	0.92	0.97	1.09	1.01			0.62	0.81	1.49

4. Conclusion

This kinetic study of furfural conversion in aqueous sulphuric acid shows that the reaction predominantly follows pseudo-first-order behaviour with respect to furfural, except for the condensation between furfural and formic acid. Furfural decomposes mainly into formic acid and humins, with reaction rates strongly influenced by acid concentration and temperature. Among the tested models, Model-3 provides the best representation of the experimental data, yielding R^2 values of 98.04% for furfural conversion and 90.35% for formic acid formation. This model accounts for condensation between furfural and the formic acid produced during its own conversion, confirming the presence of a coupled reaction network in acidic aqueous systems. The determined reaction orders of 0.81 for furfural, 0.62 for sulphuric acid, and 1.49 for formic acid indicate that formic acid plays a dominant role in accelerating humin formation, proceeding about one and a half times faster than in systems containing only furfural. Overall, the proposed kinetic framework provides a rigorous and comprehensive description of the main reaction pathways and their interactions. It offers improved predictive accuracy compared with previous models. It supplies a robust basis for optimising furfural production, controlling by-product formation, and designing more efficient acid-catalysed hydrothermal processes for biomass conversion applications.

Notation

C_{H+} = concentration of H^+
dC_F/dt = the rate of change of furfural concentration with respect to time
dC_{FA}/dt = the rate of change of formic acid concentration with respect to time
F = furfural
FA = formic acid
$k_{1,0}; k_{2,0}; k_{3,0}; k_{4,0}$ = the pre-exponential factor for reaction route-1 / route-2 / route-3/ route-4
$Ea_1; Ea_2; Ea_3; Ea_4$ = Activation energy of reaction R_1; R_2; R_3; R_4
$R_1; R_2; R_3; R_3$ = reaction rate of 1st route / 2nd route / 3rd route / 4th route
SA = sulphuric acid
X_F = furfural conversion
Y_{FA} = formic acid yield
α = order of reaction of sulphuric acid
β = order reaction of furfural
γ = order reaction of formic acid

Acknowledgment

The author gratefully acknowledges the support provided by the Master's Programme in Chemical Engineering, Parahyangan Catholic University (UNPAR). Sincere appreciation is extended to Ms Jenny N.M. Tan-Soetedjo for her invaluable supervision and guidance, and to Mr I Gede Pandega W. for his constructive suggestions and insightful contributions to the development of the kinetic modelling. The author also wishes to acknowledge the financial support received from the Research and Community Service Institute of Parahyangan Catholic University (LPPM UNPAR).

References

[1] A. R. Mankar, A. Pandey, A. Modak, and K. K. Pant, "Pretreatment of lignocellulosic biomass: A review on recent advance," Bioresource Technology, vol. 334, Aug 2021, doi: 10.1016/j.biortech.2021.125235.

[2] H. El-Gendi, E. M. El-Fakharany, M. H. El-Sayed, D. A. Alenazi, R. Jame, N. D. Alkhathami, M. A. Abdelaziz, and A. K. Saleh, "A comprehensive overview of lignocellulosic biomass exploiting for sustainable bioethanol production: recent advances and emerging challenges towards commercial implementation," Egyptian Journal of Chemistry, vol. 67, pp. 2053-2072, Oct 2024, doi: 10.21608/ejchem.2024.312880.10268.

[3] V. Menon and M. Rao, "Trends in bioconversion of lignocellulosic biofuels, platform chemicals & biorefinery concept," Progress in Energy and Combustion Science, vol. 38, no. 4, pp. 522-550, Aug 2012, doi: 10.1016/j.pecs.2012.02.002.

[4] B. Segers, P. Nimmegeers, M. Spiller, G. Tofani, E. Grojzdek, E. Dace, and P. Billen, "Lignocellulosic biomass valorisation: a review of feedstocks, processes and potential value chains and their implications for the decision-making process," RSC Sustainability, vol. 2, no. 12, pp. 3730-3749, Oct 2024, doi: 10.1039/d4su00342j.

[5] S. Swami, S. Suthar, R. Singh, A. Thakur, L. Gupta, and V. Sikarwar, "Potential of ionic liquids as emerging green solvent for the pretreatment of lignocellulosic biomass," Environmental Science and Pollution Research, vol. 31, no. 4, pp. 1-21, Jan 2024, doi: 10.1007/s11356-024-32100-y.

[6] P. Kumar, D. M. Barrett, M. J. Delwichel, and P. Stroeve, "Methods for pretreatment of lignocellulosic biomass for efficient hydrolysis and biofuel production," Ind. Eng. Chem. Res., vol. 48, no. 8, pp. 3713-3729, 2009.

[7] T.-S. Jenny N.M, H. H. v. d. Bovenkamp, R. M. Abdilla, C. B. Rasrendra, J. v. Ginkel, and H. J. Heeres, "Experimental and kinetic modeling studies on the conversion of sucrose to levulinic acid and 5-hydroxymethylfurfural using sulfuric acid in water," Ind. Eng. Chem. Res., vol. 56, no. 45, pp. 13228-13239, Jul 2017, doi: 10.1021/acs.iecr.7b01611.

[8] L. Almhofer, R. H. Bischof, M. Madera, and C. Paulik, "Kinetic and mechanistic aspects of furfural degradation," The Canadian Journal of Chemical Engineering, vol. 101, no. 4, pp. 1-17, Sep 2022, doi: 10.1002/cjce.24593.

[9] D. Edumujeze, M.-C. Fournier-Salaün, and S. Leveneur, "Production of furfural: from kinetics to process assessment," Fuel, vol. 381, pp. 1-20, Feb 2025, doi: 10.1016/j.fuel.2024.133423.

[10] G. Marcotullio and W. D. Jong, "Chloride ions enhance furfural formation from d-xylose in dilute aqueous acidic solutions," Green Chemistry, vol. 12, no. 10, pp. 1739-1746, Oct 2010, doi: 10.1039/B927424C.

[11] G. Marcotullio and W. d. Jong, "Furfural formation form d-xylose: the use of different halides in dilute aqueous acidic solutions allows for exceptionally high yields," Carbohydrate Research, vol. 346, no. 11, pp. 1291-1293, Aug 2011, doi: 10.1016/j.carres.2011.04.036.

[12] K. Lamminpaa, J. Ahola, and J. Tanskanen, "Kinetics of xylose dehydration into furfural in formic acid," Ind. Eng. Chem. Res., vol. 51, no. 18, pp. 6297-6303, Apr 2012, doi: 10.1021/ie2018367.

[13] O. Ershova, J. Kanervo, S. Hellsten, and H. Sixta, "The role of xylulose as an intermediate in xylose conversion to furfural: insights via experiments and kinetic modelling," RSC Advances, vol. 5, no. 82, pp. 66727-66737, Aug 2015, doi: 10.1039/C5RA10855A.

[14] M. Sajid, M. R. Dilshad, M. S. U. Rehman, D. Liu, and X. Zhao, "Catalytic conversion of xylose to furfural by p-Toluenesulfonic acid (pTSA) and chlorides: process optimization and kinetic modeling," Molecules, vol. 26, no. 8, pp. 1-17, Apr 2021, doi: 10.3390/molecules26082208.

[15] J. Köchermann, J. Mühlenberg, and M. Klemm, "Kinetics of hydrothermal furfural production from organosolv hemicellulose and d-xylose," Ind. Eng. Chem., vol. 57, no. 43, pp. 14417-14427, Sep 2018, doi: 10.1021/acs.iecr.8b03402.

[16] G. Yu, D. Zhao, L. Wen, S. Yang, and X. Chen, "Viscosity of ionic liquids: database, observation, and quantitative structure-properly relationship analysis," American Institute of Chemical Engineers Journal, vol. 58, no. 9, pp. 1-15, Oct 2011, doi: 10.1002/aic.12786.

[17] K. Lammimpää, J. Ahola, and J. Tanskanen, "Kinetics of furfural destruction in a formic acid medium," RSC Advances, vol. 4, no. 104, pp. 4, 60243-60248, Nov 2014, doi: 10.1039/C4RA09276G.

[18] W. Sailer-Kronlachner, C. Rosenfeld, S. Böhmdorfer, M. Bacher, J. Konnerth, T. Rosenau, A. Potthast, A. Geyer, and H. W. v. Herwijnen, "Scale-up of production of 5-hydroxymethylfurfural-rich adhesive precursors and structural features of humin side products," Biomass Conversion and Biorefinery, vol. 14, Aug 2022, doi: 10.1007/s13399-022-03200-x.

[19] B. Girisuta, L. Janssen, and H. Heeres, "A kinetic study on the decomposition of 5-hydroxymethylfurfural into levulinic and formic acid in water," Green Chemistry, vol. 8, no. 8, pp. 701-709, Aug 2006, doi: 10.1039/b518176c.

[20] M. J. Antal, J. T. Leesomboon, and W. S. Mok, "Mechanism of formation of 2-furaldehyde from d-xylose," Carbohydrate Research, vol. 217, pp. 71-85, Sep 1991, doi: 10.1016/0008-6215(91)84118-X.

[21] S. Liu, Y. Zhu, Y. Liao, H. Wang, Q. Liu, L. Ma, and C. Wang, "Advances in understanding the humins: formation, prevention, and application," Applications in Energy and Combustion Science, vol. 10, Jun 2022, doi: 10.1016/j.jaecs.2022.100062.

[22] A. Wassenberg, T. Esser, M. J. Poller, and J. Albert, "Investigation of the formation, characterization, and oxidative catalytic valorization of humins," Materials, vol. 16, no. 7, Apr 2023, doi: 10.3390/ma16072864.

[23] H. Akaike, "A new look at the statistical model identification," IEEE Transactions on Automatic Control, vol. 6, no. 19, pp. 716-723, Dec 1974, doi: 10.1109/TAC.1974.1100705.

[24] K. P. Burnham and D. R. Anderson, Model selection and multimodel inference: a practical information theoretic approach, 2nd ed. New York, USA: Springer, 2002.

[25] E. A. Mohammed, C. Naugler and B. H. Far, "Chapter 32 - emerging business intelligence framework for a clinical laboratory through big data analytics," in Emerging Trends in Computational Biology, Bioinformatics, and System Biology, pp. 577-602, 2015.

[26] J. N. Tan-Soetedjo, H. H. v. d. Bovenkamp, R. M. Abdilla, C. B. Rasrendra, J. v. Ginkel and H. J. Heeres, "Experimental and kinetic modelling studies on the conversion of sucrose to levulinic acid and 5-hydroxymethylfurfural using sulfuric acid in water," Ind. Eng. Chem. Res., vol. 56, no. 45, pp. 13228-13239, Jul 2017, doi: 10.1021/acs.iecr.7b01611.

[27] I. v. Zandvoort, Y. Wang, C. B. Rasrendra, E. R. v. Eck, P. C. Bruijnincx, H. J. Heeres, and B. M. Weckhuysen, "Formation, molecular structure, and morphology of humins in biomass conversion: influence of feedstock and processing conditions," ChemSusChem, vol. 6, no. 9, pp. 1-15, Jul 2013, doi: 10.1002/cssc.201300332.

[28] J. Carlos, V. Calderón, J. S. Arora, and S. H. Mushrif, "Mechanistic investigation into the formation of humins in acid-catalyzed biomass reaction," ACS Omega, no. 7, no. 49, pp. 44786-44795, Nov 2022, doi: 10.1021/acsomega.2c04783.

[29] E. d. Jong, M. Mascal, S. Constant, T. Claessen, P. Tosi, and A. Mija, "The origin, composition, and applications of industrial humins - a review," Green Chemistry, vol. 27, no. 12, pp. 3136-3166, Feb 2025, doi: 10.1039/d4gc06244b.

[30] K. Dussan, B. Girisuta, M. Lopes, J. J. Leahy, and M. H. Hayes, "Conversion of hemicellulose sugars catalyzed by formic acid: kinetics of the dehydration of D-xylose, L-arabinose; and D-glucose," Chem. Sus. Chem., vol. 18, no. 8, pp. 1411-1428, Mar 2015, doi: 10.1002/cssc.201403328.

[31] K. Namhaed, W. Kiatkittipong, T. Triquet, and P. Cognet, "Dehydration of pentose to furfural catalyzed by formic acid - kinetics and application to real biomass hydrolysates," Journal of Environmental Chemical Engineering, vol. 12, no. 15, Oct 2024, doi: 10.1016/j.jece.2024.113431.

[32] G. Marcotullio, W. D. Jong, M. A. T. Cardoso, and A. H. Verkooijen, "Bioenergy II: furfural destruction kinetics during sulphuric acid-catalyzed production from biomass," International Journal of Chemical Reactor Engineering, vol. 7, no. 1, Jan 2009, doi: 10.2202/1542-6580.1980.

[33] X. Li, Q. Liu, C. Luo, X. Gu, L. Lu, and X. Lu, "Kinetics of furfural production from corn cob in γ-valeroolactone using dilute sulfuric acid as catalyst," ACS Sustainable Chem. Eng., vol. 5, no. 10, pp. 8587-8593, Sep 2017, doi: 10.1021/acssuschemeng.7b00950.

[34] E. Rakić, A. Kostyniuk, N. Nikačevič, and B. Likozar, "Reaction microkinetic model of xylose dehydration to furfural over beta-zeolite catalyst," Biomass Conversion and Biorefinery, vol. 15, no. 2, pp. 2303-2317, Oct 2023, doi: 10.1007/s13399-023-04969-1.

[35] G. Tsilomelekis, M. J. Orella, Z. Lin, Z. Cheng, W. Zheng, V. Nikolakis, and D. G. Vlachos, "Molecular structure, morphology and growth mechanism and rates of 5-hydroxymethyl furfural (HMF) derived humins," Green Chemistry, vol. 18, no. 7, pp. 1983-1993, Nov 2015, doi: 10.1039/C5GC01938A.